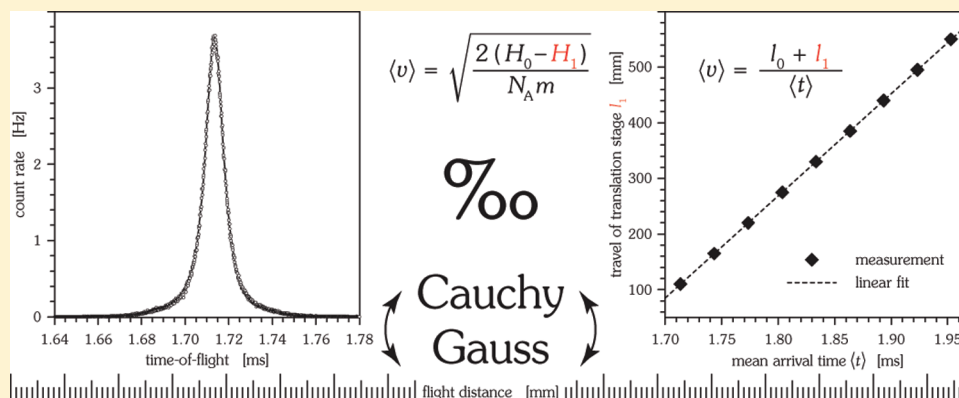# Precision Velocity Measurements of Pulsed Supersonic Jets

Wolfgang Christen,* Tim Krause, Björn Kobin, and Klaus Rademann

Institut für Chemie, Humboldt-Universität zu Berlin, Brook-Taylor-Strasse 2, 12489 Berlin, Germany

ABSTRACT:

$$\langle v \rangle = \sqrt{\frac{2\,(H_0 - H_1)}{N_A m}}$$

$$\langle v \rangle = \frac{l_0 + l_1}{\langle t \rangle}$$

We introduce a straightforward experimental approach for determining the mean flow velocity of a supersonic jet with very high precision. While time measurements easily can achieve accuracies of $\Delta t/t \leq 10^{-4}$, typically the absolute flight distances are much less well-defined. This causes significantly increased errors in calculations of the mean flow velocity and mean kinetic energy. The basic concept to improve on this situation is changing the flight distance in vacuo by precisely defined increments employing a linear translation stage. We demonstrate the performance of this method with a flight path that can be varied by approximately 15% with a tolerance of setting of 50 μm. In doing so, an unprecedented accurate value for the mean flow velocity of $\Delta v/\langle v \rangle < 3 \times 10^{-4}$ has been obtained without prior knowledge of the total distance. This very high precision in source pressure, temperature, and particle speed facilitates an improved energetic analysis of condensation processes in supersonic jet expansions. The technique is also of broad interest to other fields employing the strong adiabatic cooling of supersonic beams, in particular, molecular spectroscopy. In the presented case study, a thorough analysis of arrival time spectra of neutral helium implies cluster formation even at elevated temperatures.

INTRODUCTION

The formation and growth of clusters in the gas phase is a common phenomenon in nature and technology. The condensation of supersaturated gases also is of fundamental relevance in a number of research fields, such as, for instance, atmospheric and environmental chemistry, chemical engineering, and process technology. Recently, this subject has experienced a remarkable renaissance owing to urging questions in climate research and fascinating applications in materials science and also due to significant progress achieved in computer-based molecular simulations[1−3] and modern experimental methods.[4−7] Despite a great deal of theoretical and experimental work, open questions remain, including, for example, the gas−liquid phase transition close to the critical point and rapid nonequilibrium processes.

Quantitative techniques for investigating homogeneous nucleation and cluster growth encompass studies determining the "onset" of nucleation, critical supersaturation or nucleation rate.[6,8,9] Suitable experimental instrumentation include thermal diffusion cloud chambers where two plates are maintained at different temperatures, providing a largely linear gradient in temperature, partial vapor pressure and supersaturation.[6] The most prevalent

approach, however, is an adiabatic gas expansion. Here, a variety of sophisticated techniques has been developed, including nucleation pulse chambers[10,11] employing an expansion−compression sequence, with the aim of separating the processes of cluster formation and cluster growth. Supersonic nozzle jets permit very high transient supersaturations that can be fine-tuned via source pressure and temperature, allowing assessment of a wide parameter range from low particle densities up to and including the supercritical region. Specifically, they provide the opportunity to directly monitor cluster formation, from dimers up to droplets reaching the size of micrometers, at notably well-defined boundary conditions. In the majority of nucleation experiments, generated clusters are registered using scattered laser light. Although both single molecules and particles with diameters larger than a few nanometers can be readily detected employing nondestructive
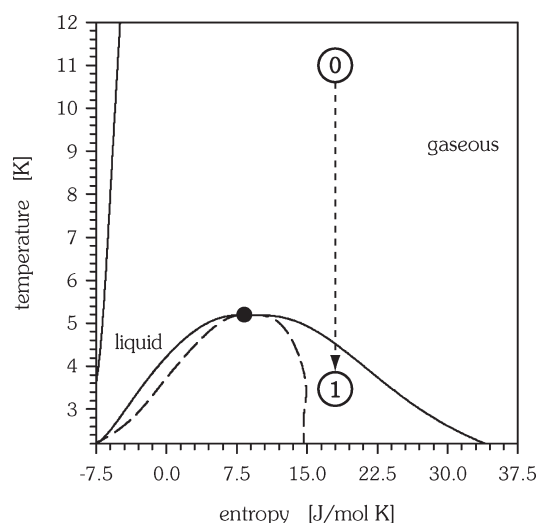
Figure 1. Schematic representation of an isentropic jet expansion, characterized by a vertical trajectory (dotted arrow), starting from supercritical source conditions (0) and reaching the metastable region (1) where condensation sets in. The exact location of (1) is difficult to access in experiments. The depicted $T-S$ phase diagram has been calculated with the most accurate equation of state of helium currently available.[35,36] The critical point is located at the temperature $T_c = 5.20$ K and the molar entropy $S_c = 8.32$ J mol^{-1} K^{-1}.

optical techniques, the intermediate size range commonly necessitates the use of mass spectrometric methods. Unfortunately, these are characterized by ionization-induced fragmentation processes obscuring the native cluster size distribution. On this account, several alternative methods have been explored, including the deflection of clusters by elastic collisions with a secondary beam,[12,13] collisions with a buffer gas,[14,15] diffraction from transmission gratings,[16] and nanoscale particle sieves.[17]

In this contribution, a precise velocity measurement is utilized as a universally practicable approach for gaining insight into the proportion of condensation in an expanded beam. Assuming an initially isentropic process (see Figure 1), the thermodynamic end state of the supersonic beam at a large distance from the nozzle can be deduced from an accurate determination of the enthalpy change, $H_0 - H_1$, realized by a measurement of the terminal flow velocity $\langle v \rangle$

$$\langle v \rangle = \sqrt{\frac{2(H_0 - H_1)}{N_A m}}$$

This description assumes identical particles each of mass m; $N_A = 6.022 \times 10^{23}$ mol^{-1} is Avogadro's constant. The center-of-mass motion of the gas within the reservoir is neglected.[18] Ensuring thermodynamic equilibrium at source pressure P_0 and source temperature T_0 and a proven equation of state (EOS) for the computation of $H(P,T)$ at hand, it is then possible to derive the change of enthalpy from a measurement of the terminal mean flow velocity. By this means, the energy balance and also important macroscopic properties of supersonic beams such as the amount of condensation can be obtained.[18]

For such studies, helium is an attractive choice because it is one of the chemically simplest but also most challenging systems, constituting, for example, the weakest bound molecule, He$_2$.[16,19−22] In cryogenic supersonic beams, it also shows pronounced real gas effects[23−27] and intriguing quantum properties such as

superfluidity.[28] As a matter of fact, helium clusters have established new research areas in low-temperature physics and spectroscopy.[29−34]

There are also several other applications of supersonic beams where the mean flow velocity of particles needs to be obtained with high accuracy, e.g. reactivity studies determining the kinetic energy transfer in gas-phase or gas−surface collisions.

Customarily, time-of-flight (TOF) methods are used for a velocity and kinetic energy analysis. In this contribution, we demonstrate a straightforward possibility for obtaining flow velocities with very high precision. This way, the accuracy of state-of-the-art experiments can be further improved by at least 1 order of magnitude. The much reduced uncertainties allow discriminating between different model descriptions and contributions to an improved comprehension of real gas effects.

■ EXPERIMENTAL METHOD

The average flow velocity $\langle v \rangle$ of a supersonic beam can be determined using established time-of-flight methods.[37] In such experiments, the arrival time distribution (ATD) of a bunch of particles passing from a source position at a time t_1 to the position of a detector at a mean arrival time $\langle t_2 \rangle$ is measured. Subject to the knowledge of the distance l between the source and detector, the mean particle speed can be calculated

$$\langle v \rangle = \frac{l}{\langle t_2 \rangle - t_1}$$

This approach assumes a linear movement and a uniform flow velocity. Both conditions are fulfilled for horizontally aligned flight paths and neutral particles, permitting the neglect of acceleration caused by electric, magnetic, and gravitational fields.

Despite this simple concept, the exact distance traveled may be hard to determine in practice. It is quite demanding, for example, to exactly locate the ionization volume of an electron source in a mass spectrometer. Likewise, the use of bellows or gaskets of varying thickness in vacuum systems tends to deteriorate accuracy. Accordingly, in many cases, the largest uncertainty in determining the mean flow velocity or mean kinetic energy of a molecular beam is caused by an ill-defined length of the flight path between the source and detector.

A general and very accurate solution for the determination of the mean beam velocity even in cases where the distance is not known at all is made possible by changing the length in accurately defined units. This can be realized by applying a precision translation stage. The total flight distance $l = l_0 + l_1$ then is composed of a constant, unknown length l_0 and a very accurately defined, variable length l_1, which is provided by the translation stage. Repeated ATD measurements at several different values of l_1 will yield a corresponding set of mean arrival times $\langle t_2 \rangle$. These data can be numerically evaluated by a linear least-squares fit revealing both the mean flow velocity $\langle v \rangle$ and the residual distance l_0.

TOF experiments require a means of modifying beam properties in order to mark time zero, t_1. While customarily, mechanical choppers are used for this purpose, in an ultrahigh vacuum (UHV) environment, a rapidly rotating disk raises considerable technical issues. Alternative approaches are facilitated by using fast pulsed nozzles.[38,39] In both cases, however, the temporal resolution is limited due to a comparatively long modulation time of tens of microseconds. For noble gas atoms and a few molecules with long-lived metastable states, a pulsed electron beam may serve as a fast electronic chopper,[40] tagging spatially and temporally

B

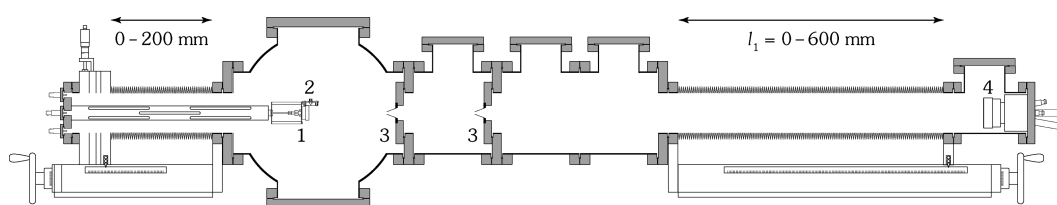dx.doi.org/10.1021/jp112222g |*J. Phys. Chem. A* XXXX, XXX, 000–000

Figure 2. Schematics of the experimental setup. (1) Pulsed, temperature- and pressure-controlled supersonic jet source mounted on a *xyz*-translation stage. (2) Pulsed electron gun for electronic excitation of noble gas atoms, located approximately 5 mm in front of the valve. The focused electron beam is directed perpendicularly to the axis of the expanding gas jet, with an electron energy of 140 ± 1 eV. (3) Conical skimmers with diameters of 3 and 2 mm. (4) Electrically shielded time-of-flight detector, mounted on a linear translation stage.

selected particles at a time resolution of a few hundred nanoseconds. Collisions of these electronically excited species lead to a very efficient de-excitation into the ground state, either by resonance ionization followed by Auger neutralization or by Auger de-excitation.[41] For helium, the two lowest-lying excited levels are both long-lived with a lifetime of 19.7×10^{-3} s for the $2\ {}^1S_0$ state[42] and 7.9×10^3 s for the $2\ {}^3S_1$ state,[43] respectively; hence, these atoms remain in the metastable levels until they are collisionally de-excited just in front of the detector surface. The de-excitation may result in the emission of secondary electrons providing a measure of the metastable flux;[44] it can be detected by a multichannel plate (MCP) with grounded input surface.

■ EXPERIMENTAL REALIZATION AND PRECISION

In the experiments presented here, a pulsed valve[45] with an adjustable opening time is combined with metastable tagging, resulting in a bunch of electronically excited helium atoms with an initial pulse duration of 500 ns. Although pulse widths as short as 100 ns are possible, there is a trade-off in signal intensity, adversely affecting counting statistics.

Figure 2 depicts essential elements of the general setup, and Figure 3 details the timing scheme for ATD measurements. A cold supersonic helium beam is generated using a high-pressure jet expansion through an electromagnetic pulsed valve,[38,45] featuring a highly polished trumpet-shaped nozzle with an opening diameter of 0.1 mm. The temperature is measured using a NiCr/Ni thermocouple spot-welded to the exterior of the valve.[45] The readings of the thermocouple have been standardized against a calibrated precision thermometer, resulting in an absolute temperature error of 0.20 K at most. The pressure in the gas supply line is measured by means of an ultrahigh precision pressure transducer with a maximum error of 10 kPa.[46] Proportional integral derivative control algorithms are used for driving a pulseless syringe pump fine-tuning the gas pressure in the reservoir and a circulator maintaining the valve temperature. Evaluating the temperature of the heat-transfer oil that is continuously streaming through the valve body yields valuable information about residual temperature gradients and thermal equilibrium within the valve. These efforts permit keeping the relevant thermophysical parameters constant within a bandwidth of ± 1 kPa and ± 25 mK.

The pulsed valve is mounted on a *xyz*-translation stage, allowing for both horizontal and vertical alignment of the propagating jet with respect to the molecular beam axis, defined by two conical skimmers. Moreover, the distance between the valve and first skimmer can be changed in vacuo, increasing the standard value by a maximum of 200 mm. This property is of particular relevance for high-density jet expansions where particle scattering at the skimmer may severely affect beam quality.
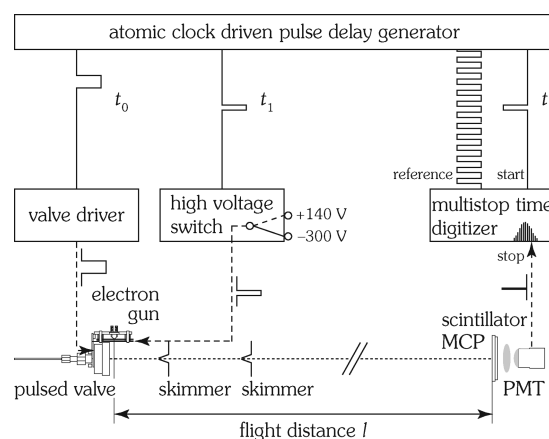

Figure 3. Timing scheme for the measurement of arrival time distributions in pulsed supersonic jet experiments. A digital delay/pulse generator (Stanford Research Systems DG645) with a rubidium time base synchronizes data acquisition and control of the experiment. It is characterized by a phase jitter of 30 ps and an absolute temporal accuracy of 1 ns. The time origin of TOF spectra is defined through the pulsed electron beam excitation. The respective electrode voltage of the electron source is changed using a high-voltage push−pull switching unit (Behlke GHTS 30) with a turn-on jitter of 100 ps. At the detector surface, metastable He atoms generate stop events that are precisely counted in the exact relation to their arrival time using an ultrafast time digitizer (FAST P7887) with a native time resolution of 250 ps.

Accordingly, in the experiments reported here, a long distance of 176 mm between the nozzle and first skimmer is used.

Throughout this work, the repetition rate of the pulsed valve is 2.2 Hz, resulting in a maximum working pressure in the first chamber of 2.0×10^{-4} Pa (already corrected for detection efficiency of the cold cathode gauge). By this means, the number of particle collisions with background gas is minimized.

Helium gas with a specified purity of 99.999% is expanded into vacuum and partially excited into metastable states employing a pulsed electron beam. Owing to a narrow acceptance angle of the detector of 0.03°, defined by the two skimmers, and the high excitation energy of He*, only resonantly excited helium can be detected.[40,47−50] The interaction volume of the electron beam and molecular beam has been optimized by adapting the focusing voltages of the electron gun optics.

Separated by differential pumping stages, the last UHV chamber (operation pressure of $<3 \times 10^{-7}$ Pa) provides a TOF detector. It is mounted on a rigid linear translation stage, offering maximum positional stability together with travel of up to 600 mm. The kinetic energy of helium ions impacting the detector surface is not sufficient to generate secondary electrons. Hence, besides energetic photons only electronically excited, neutral He atoms

are registered. The output signal is electro-optically isolated using a sequence of MCP, scintillator, and photomultiplier tube (PMT) (see Figure 3) and characterized by a rise time of less than 1 ns. Pulses are counted with a temporal resolution of 250 ps.

In TOF spectrometry, events resulting primarily from the detection of sufficiently energetic photons or particles are recorded as a function of time. Owing to digitalized data processing, the time axis is split into short intervals of equal length. For negligible dead times and sufficiently low event rates, the measurements exhibit statistical fluctuations that are described by the Poisson probability distribution.[52] The finite period of the counting intervals and the total number of events within a peak affect the precision of determining the peak position. Typically, the centroid of the peak is utilized to define the peak position and to provide a measure of the mean arrival time $\langle t_2 \rangle$. For any arbitrary peak shape, the standard deviation of the centroid σ_c is given by

$$\sigma_c = \frac{\sigma}{\sqrt{N}}$$

N is the number of all events contributing to the peak, that is, the peak area, and σ is the standard deviation of the mean. Because for narrow distributions with a large number of events the resulting error in the estimated peak position is minimized, the experiments have been performed at a high source pressure. For noble gases at elevated temperatures, these conditions result in both abundant particles and considerably increased translational cooling, ensuring ultrasharp peaks in the TOF spectra. Figure 4 depicts a representative TOF measurement. Typical values of spectra used in this work are a peak width of $\sigma = 5$ μs and an intensity of $N = 3.9 \times 10^5$ counts, resulting in an uncertainty of the mean arrival time $\langle t_2 \rangle$ of 8 ns. In comparison, the centroid error caused by the temporal width of the sampling periods of 128 ns is smaller by many orders of magnitude[52] and thus can be safely neglected.

Because the experimental definition of the mean flight time from the source to the detector actually implies the determination of a time difference, $\langle t_2 \rangle - t_1$, the accuracy of the zero point on the time scale, t_1, also affects overall TOF precision. This temporal origin of the spectra is defined by the center of the electronic excitation pulse, t_1 (see Figure 3). Hence, while the duration of the electron beam pulse slightly increases the width of the ATD of the tagged He beam, it does not affect the center position. Moreover, photons emitted during the pulsed electron beam operation and arising from the decay of short-lived ($\sim 10^{-8}$ s) Rydberg states[51] are detected too (see inset of Figure 4A), permitting validation of the zero point and the absence of any intrinsic delays with an accuracy of one sampling period. For that reason, the photon peak has been measured separately with an interval width of 16 ns. For comparison, the flight time of the photons from the source position to the detector amounts to ~ 11 ns.

In summary, the hardware-based timing error is rated as 16 ns, twice as large as the uncertainty of 8 ns resulting from counting statistics. In comparison, consideration of the finite lifetime of the helium $2\ ^1S_0$ state of 19.7 ms shifts the mean arrival time by less than 2 ns.

■ DATA EVALUATION AND PRECISION

The process of determining parameters of the statistical arrival time distribution also contributes to the overall uncertainty of the
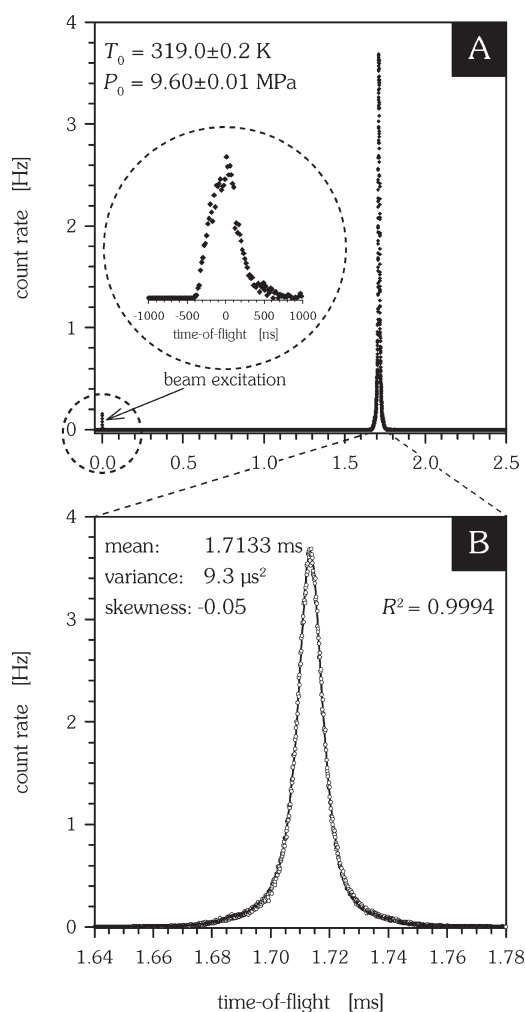

Figure 4. Arrival time distribution of a pulsed supersonic beam of metastable helium. A: The temporal origin, t_1, is defined by pulsed electron beam excitation (pulse length of 500 ns) and corroborated by the detection of energetic photons (inset). B: Detailed view of the ATD peak shape, results of a method of moments evaluation, and least-squares fit of Student's t probability distribution, yielding a coefficient of determination of $R^2 > 0.999$.

mean flight time. Mathematical procedures for estimating population parameters from sample statistics are maximum likelihood, least-squares, method of moments, and others. Comparing results of these techniques yields a reliable evaluation of the errors involved in data analysis.

The first moment as the weighted average of a sample distribution is frequently used to describe the mathematical expectation of the mean arrival time, $\langle t_2 \rangle$, while the variance, σ^2, as a measure of the peak width is given by the second central moment. The third central moment is a measure of skewness, that is, the asymmetry of a probability distribution, and can be estimated as

$$m_3 = \frac{\sum_{i=1}^{n} y_i (t_i - \bar{t})^3}{\sum_{i=1}^{n} y_i}$$

where n denotes the number of counting intervals, y_i the number of counts in interval i, and $\bar{t}$ the sample mean. Figure 4B shows a

detailed view of a typical He* peak shape, including numeric values of standardized central moments, and a least-squares fit of Student's t distribution. Obviously, skewness is rather small and evidence for a highly symmetric distribution function. Indeed, the mean and median of all TOF spectra of this investigation differ by less than 210 ns. Accordingly, one may be tempted to fit the spectra with symmetric probability distribution functions.

Frequently, a Gaussian (or normal) distribution

$$f(t, a, b) \, dt = \frac{1}{\sqrt{2\pi}b} \exp\left[-\frac{1}{2}\left(\frac{t - a}{b}\right)^2\right] dt$$

is used as a first approximation, with location parameter a and scale parameter b. The mean arrival time is given by $\langle t_2 \rangle = a$ and the full width at half-maximum (fwhm) of the peak by $\delta t = 2(2 \ln 2)^{1/2}b$. In related work, also a Lorentzian (or Cauchy) distribution

$$f(t, a, b) \, dt = \frac{b}{\pi[(t - a)^2 + b^2]} \, dt$$

has been considered.[22,53] This probability density function much better accounts for broad peak tails, which are also observed here (see Figure 4B). In optical spectroscopy, homogeneous broadening yields a Lorentzian line shape, while inhomogeneous broadening results in a Gaussian profile. In supersonic beams of electronically excited helium from high-density jet expansions, similar mechanisms might be effective, that is, excited-state complex (Rydberg matter cluster) formation, energy transfer, or collisional quenching, resulting in a Lorentzian-like profile. In view of the experimental setups employed to measure arrival times,[22,53] however, thus far, no physical justification for applying such a probability distribution has been offered.

Mathematically, both distribution functions are special cases of the noncentral Student t probability distribution

$$f(t, a, b, c) \, dt = \frac{\Gamma\left(\dfrac{c + 1}{2}\right)}{\sqrt{c\pi}b\Gamma\left(\dfrac{c}{2}\right)}\left[1 + \frac{(t - a)^2}{cb^2}\right]^{-(c+1)/2} dt$$

providing an additional shape parameter, c. For $c = 1$, the t distribution is mathematically equivalent to a Cauchy distribution, while for $c \rightarrow \infty$, it is numerically identical to a normal distribution.

In all TOF spectra of this investigation, the statistical correlation between experimental data and the least-squares fit of a model Student t distribution function is excellent, with the coefficient of determination

$$R^2 = 1 - \frac{\displaystyle\sum_{i=1}^{n}(y_i - f_i)^2}{\displaystyle\sum_{i=1}^{n}(y_i - \bar{y})^2} \geq 0.999$$

Here, f_i denotes fit values and $\bar{y}$ the mean of the experimental count numbers. Due to a very symmetrical line shape, the application of different distribution functions, that is, Gaussian, Lorentzian, and Student's t, yields identical results within a maximum difference of the centroid positions of 45 ns.

Stimulated by the hitherto unexplained observation of Lorentzian-like line shapes, also a fit of two Gaussian distribution functions has been conducted. As an example, the fit of one
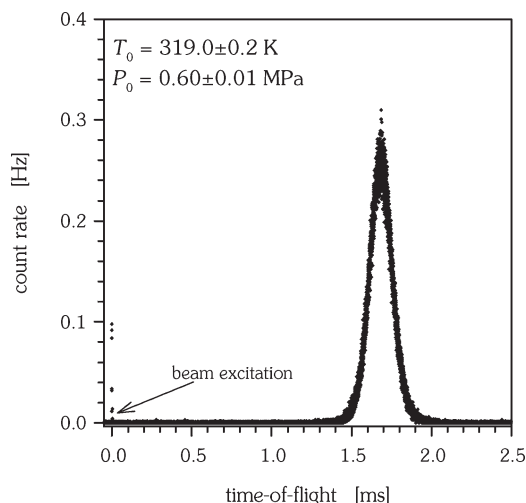

Figure 5. Arrival time distribution of a pulsed supersonic beam of metastable helium at a source pressure of $P_0 = 0.60$ MPa, characterized by a mean arrival time of 1.7168 ms and a variance of 98.7 μs^2. Obviously, the peak shape resembles a Gaussian distribution function, with a coefficient of determination of $R^2 = 0.993$ as compared to $R^2 = 0.994$ for Student's t distribution. Although the flight distance is identically equal to the spectrum depicted in Figure 4, the mean arrival time is larger by 2%.

Gaussian distribution function of the spectrum depicted in Figure 4 yields a coefficient of determination of $R^2 = 0.983$ and of 0.998 for two Gaussian distribution functions. The latter agreement compares well with the fit result of $R^2 = 0.997$ for one Lorentzian distribution and of $R^2 = 0.999$ for one Student's t distribution. Thus, this observation is reminiscent of a condensed, narrow, and a less cold, broader fraction of helium atoms, as has been reported, for example, in ref 54.

Considering the finite value of the skewness, also asymmetric probability distribution functions have been fitted to the ATD spectra. Besides Maxwell−Boltzmann,[60] noncentral Gamma

$$f(t, a, b, c) \, dt = \frac{1}{b\Gamma(c)}\left(\frac{t - a}{b}\right)^{c-1} \exp\left[-\frac{t - a}{b}\right] dt$$

and Weibull distributions

$$f(t, a, b, c) \, dt = \frac{c}{b}\left(\frac{t - a}{b}\right)^{c-1} \exp\left[-\left(\frac{t - a}{b}\right)^c\right] dt$$

have been utilized. However, the accuracy of fit of these model functions did not match the quality of Student's t distribution by far.

It is quite interesting to note that source pressure not only affects peak width as a measure of translational cooling but also peak shape. For example, at a more common stagnation pressure of $P_0 = 0.6$ MPa, the ATD is much closer to a Gaussian distribution function; see Figure 5. This dramatic change in line shape from Gaussian-like to Lorentzian-like is tentatively attributed to the formation of helium clusters at elevated pressures. The proposition is supported by the fact that also the mean arrival time is higher, monotonously decreasing with increasing stagnation pressure, as is expected from a real gas calculation.[18]

At this level of experimental accuracy, three frequently overlooked aspects are to be considered in data analysis.

First, counting systems suffer from missed events due to detector (and electronics) dead times and possibly simultaneously

E

arriving particles. Because the probability of coarriving particles is distributed according to Poisson statistics, at sufficiently low event rates, this nonlinearity can be corrected numerically.[55,56] For the TOF spectra reported here, the extensible detector dead time of 1.5 ns and the decidedly very low event count densities of less than 3.3×10^{-3} counts per interval and sweep yield a maximum correction factor of count numbers of 1.005. This correction increases the peak intensity by up to 5 ‰, reduces peak width by up to 10 ns, and affects the mean arrival time by less than 1 ns.

Second, fitting counted events in histograms using the familiar method of least-squares is appropriate only for Gaussian distributions.[57] For any other model function, a suitable maximum likelihood estimator $\Pi_{i=1}^{n} f(t_i, a, b, c)$ is required for a strictly correct evaluation. Here, the best fit of a model distribution is given by parameters maximizing the log-likelihood function instead of minimizing the sum of the squared residuals. In the case of symmetric functions, the two evaluation methods yield different values for the width of the distribution, while for asymmetric functions, also the peak position is affected. Due to the high symmetry of the helium TOF spectra, maximum likelihood estimation and least-squares optimization result in centroid positions which differ by less than 60 ns.

Third, numeric evaluation of TOF spectra necessitates the assignment of a time axis. In the majority of cases, the time value ascribed to a histogram interval is implicitly assumed to correspond to the center of this interval. Obviously, this involves time errors as large as one interval width. This prevalent mistake can be readily avoided by fitting cumulative distribution functions to cumulated data.[56] Indeed, cumulative fit functions yield mean arrival times that are markedly different from conventional probability density function fits, with deviations as large as one interval width.

In summary, the entire data evaluation procedure adds a mean error in arrival times of 220 ns and a maximum uncertainty of 315 ns. Even for the shortest distance with a flight time of 1.7 ms, this corresponds to an accuracy of 1.3×10^{-4}. Because the mean flow velocity is evaluated as the change of flight times with changing distance, any constant temporal error in measurement will only affect the accuracy of the total flight length.

■ RESULTS AND DISCUSSION

Owing to the greatly reduced duty cycle, pulsed nozzles may strongly decrease the gas load in vacuum systems, simultaneously providing a favorable means of beam modulation. Because of the restricted opening time, the particle density in the expanding jet initially increases and shortly afterward decreases again, resulting in a varying number of particle−particle collisions. As a consequence, the velocity distribution may also change, affecting, most notably, translational cooling and cluster formation.

This time dependence of beam properties can be characterized in detail by systematically shifting the time delay between triggering of the valve and metastable beam excitation, $t_1 - t_0$; see Figure 3. By this means, any part of the pulsed supersonic beam can be measured with respect to the relative intensity, mean arrival time, and spread of arrival times. In particular, this delay time scan permits determination of the central part of the beam where stationary conditions are predicted to prevail.[58,59] A corresponding set of measurements is shown in Figure 6 for He* at a source temperature of 319.0 ± 0.2 K and a stagnation pressure of 9.60 ± 0.01 MPa. Each data point in this figure has been obtained
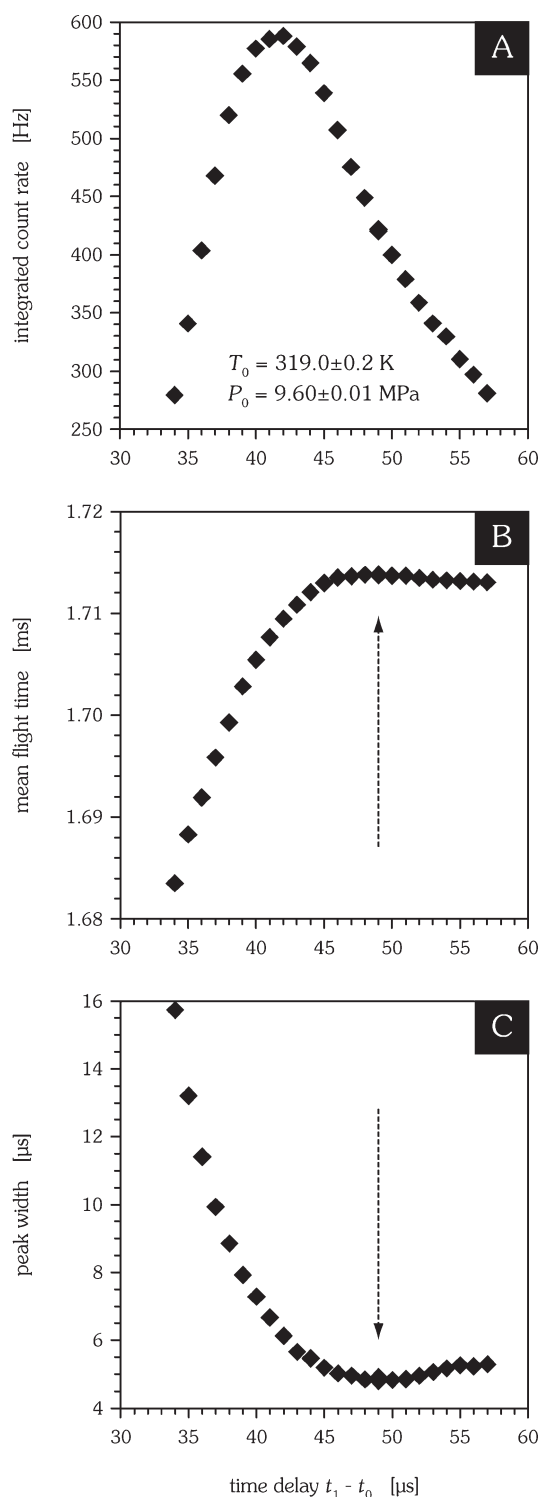

Figure 6. Characteristic properties of the pulsed He* jet, obtained by changing the time delay $t_1 - t_0$ between triggering the high voltage switch and the valve driver. A: Temporal intensity profile. B: Mean flight time $\langle t_2 \rangle - t_1$. C: Peak width σ. The dashed arrows indicate the delay time chosen for the determination of the mean flow velocity.

by summing all counts of a given TOF spectrum in the time range from 1.2 to 3.0 ms and subtracting the (few) offset counts.

From the intensity profile (Figure 6A), the actual duration of the molecular beam pulse at a distance of a few millimeters from
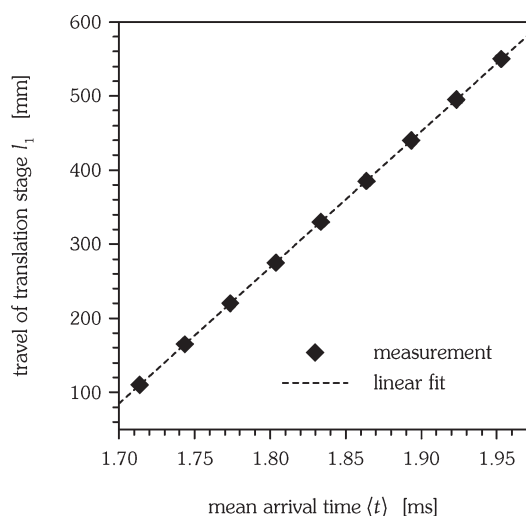
Figure 7. Mean arrival time $\langle t_2 \rangle - t_1$ of the tagged He pulse as a function of the translation stage travel. For nine distance settings of the translation stage, six arrival time measurements each are used to derive a linear correlation. The average standard error in arrival times is 32 ns. The linear regression using the depicted 9×6 data points yields a mean flow velocity of $\langle v \rangle = 1837.65 \pm 0.53$ ms^{-1} and a constant flight distance of $l_0 = 3038.8 \pm 1.0$ mm.

the valve can be derived. The fwhm of the jet amounts to approximately 20 μs. Considering the velocity spread of the beam, this value correlates quite well with the nominal opening time of the valve of 16 μs that has been set at the driver.

The smallest peak widths are observed for time delays of 46–52 μs, that is, shortly after the maximum intensity of excited He atoms is reached; see Figure 6C. In this section of the beam, translational cooling is most efficient. The appropriate experimental measure for this property is the speed ratio S, which is defined by the ratio of the mean flight time $\langle t \rangle = \langle t_2 \rangle - t_1$ to the fwhm of the ATD, δt.

$$S = 2\sqrt{\ln 2} \cdot \frac{\langle t \rangle}{\delta t}$$

The corresponding part of the beam is characterized by a speed ratio of $S = 295 \pm 5$, equivalent to an energy resolution of 0.2 meV at $E_{kin} = 60$ meV. The value of the speed ratio can be converted into an estimate of the translational temperature,[60] yielding $T_{\parallel} \simeq 9$ mK.

Also in this time range, the mean arrival time is nearly constant, changing by only 52 ns for delay times between 48 and 51 μs; see Figure 6B. Hence, for these settings, any jitter of the valve opening will keep variations of the mean arrival time to a minimum. Taking into account the beam characteristics, a time delay of 49 μs is particularly suitable for a precise determination of the mean flow velocity, despite the reduced intensity; in Figure 6, this delay time is marked by an arrow.

For a total of nine different settings of the detector translation stage, multiple ATD measurements are conducted. For each distance of l_1, six TOF spectra are evaluated; the resulting arrival times are displayed in Figure 7. The "inverse" graphic representation permits the fit of the linear function

$$l_1 = \langle v \rangle (\langle t_2 \rangle - t_1) - l_0$$

The numerical regression of this equation yields a mean flow velocity of $\langle v \rangle = 1837.7 \pm 0.5$ ms^{-1} and, simultaneously, a

constant flight distance of $l_0 = 3038.8 \pm 1.0$ mm. The specified error results from conducting several measurements. In comparison, the combined temporal error in the arrival time is smaller by a factor of 2. An analogous contribution to the remaining uncertainty in the mean flow velocity arises from the overall thermal stability of the reservoir; during the complete series of measurements, the largest temperature fluctuation encountered amounts to 45 mK. For an isentropic jet expansion of He at $T_0 = 319$ K and $P_0 = 9.6$ MPa, a change of source temperature of ± 0.045 K affects the mean terminal flow velocity by ± 0.14 ms^{-1}. In comparison, the effect of pressure stability can be safely neglected; for helium at $T_0 = 319.0$ K, a change of 1 kPa at a stagnation pressure of 9.6 MPa affects the mean flow velocity by 0.0018 ms^{-1}. Similarly, the divergence of the molecular beam as defined by the second skimmer (diameter of 2.0 mm) located at a distance of 379 mm to the nozzle contributes on the order of 0.007 ms^{-1}.

The achieved long-term accuracy means that the stability of the complete experimental system is significantly better than 3×10^{-4}. This result is crucial for calibration methods requiring constant and strictly reproducible molecular beam parameters.

The mean flow velocity of $\langle v \rangle = 1837.7$ ms^{-1} obtained experimentally may be compared to the theoretical prediction of an isentropic jet expansion of an ideal gas of 1820.1 ms^{-1}. Using a "good" standard velocity resolution of 2%, these two values could not be distinguished. Obviously, at such high source pressures, the early release of condensation energy into the beam leads to an increased flow velocity.[18] Interestingly, this helium cluster formation does not significantly increase the translational temperature; the values obtained in this work are 1 order of magnitude lower than has been reported previously[53] under comparable experimental conditions.

In this contribution, both a pressure dependence of the mean flow velocity of helium at elevated temperatures and a dramatic change of the ATD peak shape with source pressure are reported for the first time. These observations are made possible only by an unprecedented accuracy in experimental methodology and numeric data evaluation. They strongly suggest the formation of helium clusters in the beam. Interestingly, even the most advanced EOS for helium,[35] as depicted in Figure 1, claims an accuracy of only a few percent at cryogenic temperatures. Accordingly, the EOS does not indicate cluster formation for source conditions investigated in this and other related work. Highly precise studies of supersonic jet expansions might thus also help to significantly improve the accuracy of thermophysical properties.

■ SUMMARY

Combining an advanced temperature and pressure control of the stagnation reservoir with a precisely adjustable flight length permits the generation of supersonic molecular beams with an extremely well characterized velocity distribution. In particular, this method provides the possibility to determine the mean terminal flow velocity of supersonic beams with unprecedented accuracy, allowing one to distinguish between different theoretical model descriptions. The key idea of this approach is to replace an unknown or imprecise distance by a precisely defined distance change. In the measurements reported here, the velocity of a tagged beam of electronically excited helium has been determined to be $\langle v \rangle = 1837.7 \pm 0.5$ m/s, corresponding to a precision of better than 3×10^{-4}. The resolution of 1 mm obtained for the constant flight path of $l_0 = 3.039$ m corresponds well with the

G

dx.doi.org/10.1021/jp112222g | J. Phys. Chem. A XXXX, XXX, 000–000

spatial extent of the electronic excitation. This achievement in kinetic energy resolution permits monitoring the minutest temperature and pressure changes in the reservoir. It thus provides one important prerequisite for precise and reliable studies of fluid-phase transitions using supersonic beams.[18,61]

■ AUTHOR INFORMATION

Corresponding Author
*E-mail: christen@wolfgang-christen.net.

■ ACKNOWLEDGMENT

■ REFERENCES

(1) Kathmann, S. M.; Schenter, G. K.; Garrett, B. C.; Chen, B.; Siepmann, J. I. *J. Phys. Chem. C* **2009**, *113*, 10354.

(2) Zhong, J.; Moghe, N.; Li, Z.; Levin, D. A. *Phys. Fluids* **2009**, *21*, 036101.

(3) Jansen, R.; Wysong, I.; Gimelshein, S.; Zeifman, M.; Buck, U. *J. Chem. Phys.* **2010**, *132*, 244105.

(4) Ghosh, D.; Manka, A.; Strey, R.; Seifert, S.; Winans, R. E.; Wyslouzil, B. E. *J. Chem. Phys.* **2008**, *129*, 124302.

(5) De Dea, S.; Miller, D. R.; Continetti, R. E. *J. Phys. Chem. A* **2009**, *113*, 388.

(6) Brus, D.; Ždímal, V.; Uchtmann, H. *J. Chem. Phys.* **2009**, *131*, 074507.

(7) Sipilä, M.; Berndt, T.; Petäjä, T.; Brus, D.; Vanhanen, J.; Stratmann, F.; Patokoski, J.; Mauldin, R. L.; Hyvärinen, A.; Lihavainen, H.; Kulmala, M. *Science* **2010**, *327*, 1243.

(8) Heist, R. H.; He, H. *J. Phys. Chem. Ref. Data* **1994**, *23*, 781.

(9) Anisimov, M. P.; Fominykh, E. G.; Akimov, S. V.; Hopke, P. K. *Aerosol Sci.* **2009**, *40*, 733.

(10) Wagner, P. E.; Strey, R. *J. Phys. Chem.* **1981**, *85*, 2694.

(11) Iland, K.; Wölk, J.; Strey, R.; Kashchiev, D. *J. Chem. Phys.* **2007**, *127*, 154506.

(12) Buck, U.; Meyer, H. *Phys. Rev. Lett.* **1984**, *52*, 109.

(13) Lewerenz, M.; Schilling, B.; Toennies, J. P. *Chem. Phys. Lett.* **1993**, *206*, 381.

(14) Cuvellier, J.; Meynadier, P.; de Pujo, P.; Sublemontier, O.; Visticot, J. P.; Berlande, J.; Lallement, A.; Mestdagh, J. M. *Z. Phys. D* **1991**, *21*, 265.

(15) De Martino, A.; Benslimane, M.; Châtelet, M.; Crozes, C.; Pradère, F.; Vach, H. *Z. Phys. D* **1993**, *27*, 185.

(16) Schöllkopf, W.; Toennies, J. P. *Science* **1994**, *266*, 1345.

(17) Schöllkopf, W.; Toennies, J. P.; Savas, T. A.; Smith, H. I. *J. Chem. Phys.* **1998**, *109*, 9252.

(18) Christen, W.; Rademann, K.; Even, U. *J. Phys. Chem. A* **2010**, *114*, 11189.

(19) Luo, F.; McBane, G. C.; Kim, G.; Giese, C. F.; Gentry, W. R. *J. Chem. Phys.* **1993**, *98*, 3564.

(20) Luo, F.; Giese, C. F.; Gentry, W. R. *J. Chem. Phys.* **1996**, *104*, 1151.

(21) Grisenti, R. E.; Schöllkopf, W.; Toennies, J. P.; Hegerfeldt, G. C.; Köhler, T.; Stoll, M. *Phys. Rev. Lett.* **2000**, *85*, 2284.

(22) Bruch, L. W.; Schöllkopf, W.; Toennies, J. P. *J. Chem. Phys.* **2002**, *117*, 1544.

(23) Buchenau, H.; Knuth, E. L.; Northby, J.; Toennies, J. P.; Winkler, C. *J. Chem. Phys.* **1990**, *92*, 6875.

(24) Scheidemann, A.; Toennies, J. P.; Northby, J. A. *Phys. Rev. Lett.* **1990**, *64*, 1899.

(25) Buchenau, H.; Toennies, J. P.; Northby, J. A. *J. Chem. Phys.* **1991**, *95*, 8134.

(26) Harms, J.; Toennies, J. P.; Knuth, E. L. *J. Chem. Phys.* **1997**, *106*, 3348.

(27) Pedemonte, L.; Tatarek, R.; Bracco, G. *Rev. Sci. Instrum.* **2003**, *74*, 4404.

(28) Grebenev, S.; Toennies, J. P.; Vilesov, A. F. *Science* **1998**, *279*, 2083.

(29) Hartmann, M.; Miller, R. E.; Toennies, J. P.; Vilesov, A. F. *Science* **1996**, *272*, 1631.

(30) Toennies, J. P.; Vilesov, A. F. *Annu. Rev. Phys. Chem.* **1998**, *49*, 1.

(31) Callegari, C.; Lehmann, K. K.; Schmied, R.; Scoles, G. *J. Chem. Phys.* **2001**, *115*, 10090.

(32) Dalfovo, F.; Stringari, S. *J. Chem. Phys.* **2001**, *115*, 10078.

(33) Toennies, J. P.; Vilesov, A. F. *Angew. Chem., Int. Ed.* **2004**, *43*, 2622.

(34) Stienkemeier, F.; Lehmann, K. K. *J. Phys. B* **2006**, *39*, R127.

(35) Ortiz-Vega, D. O.; Hall, K. R.; Arp, V. D.; Lemmon, E. W. *Int. J. Thermophys.* **2010**, to be published.

(36) Lemmon, E. W.; Huber, M. L.; McLinden, M. O. *NIST Standard Reference Database 23*; National Institute of Standards and Technology; Gaithersburg, MD, 2010.

(37) Auerbach, D. J. In *Atomic and Molecular Beam Methods*; Scoles, G., Ed.; Oxford University Press: New York, 1988.

(38) Even, U.; Jortner, J.; Noy, D.; Lavie, N.; Cossart-Magos, C. *J. Chem. Phys.* **2000**, *112*, 8068.

(39) Irimia, D.; Dobrikov, D.; Kortekaas, R.; Voet, H.; van den Ende, D. A.; Groen, W. A.; Janssen, M. H. M. *Rev. Sci. Instrum.* **2009**, *80*, 113303.

(40) Freund, R. S.; Klemperer, W. *J. Chem. Phys.* **1967**, *47*, 2897.

(41) Conrad, H.; Ertl, G.; Küppers, J.; Sesselman, W.; Haberland, H. *Surf. Sci.* **1980**, *100*, L461.

(42) Van Dyck, R. S., Jr.; Johnson, C. E.; Shugart, H. A. *Phys. Rev. A* **1971**, *4*, 1327.

(43) Hodgman, S. S.; Dall, R. G.; Byron, L. J.; Baldwin, K. G. H.; Buckman, S. J.; Truscott, A. G. *Phys. Rev. Lett.* **2009**, *103*, 053002.

(44) Dunning, F. B.; Rundel, R. D.; Stebbings, R. F. *Rev. Sci. Instrum.* **1975**, *46*, 697.

(45) Christen, W.; Rademann, K. *Rev. Sci. Instrum.* **2006**, *77*, 015109.

(46) Christen, W.; Krause, T.; Rademann, K. *Rev. Sci. Instrum.* **2007**, *78*, 073106.

(47) Pearl, J. C.; Donnelly, D. P.; Zorn, J. C. *Phys. Lett. A* **1969**, *30*, 145.

(48) Rundel, R. D.; Dunning, F. B.; Stebbings, R. F. *Rev. Sci. Instrum.* **1974**, *45*, 116.

(49) Brutschy, B.; Haberland, H. *J. Phys. E* **1977**, *10*, 90.

(50) Kohlhase, A.; Kita, S. *Rev. Sci. Instrum.* **1986**, *57*, 2925.

(51) von Haeften, K.; Laarmann, T.; Wabnitz, H.; Möller, T. *J. Phys. B* **2005**, *38*, S373.

(52) Gedcke, D. A. *Ortec Application Note AN58*; Ortec: Oak Ridge, TN.

(53) Hillenkamp, M.; Keinan, S.; Even, U. *J. Chem. Phys.* **2003**, *118*, 8699.

(54) Tychkov, A. S.; Jeltes, T.; McNamara, J. M.; Tol, P. J. J.; Herschbach, N.; Hogervorst, W.; Vassen, W. *Phys. Rev. A* **2006**, *73*, 031603.

(55) Stephan, T.; Zehnpfennig, J.; Benninghoven, A. *J. Vac. Sci. Technol., A* **1994**, *12*, 405.

(56) Titzmann, T.; Graus, M.; Müller, M.; Hansel, A; Ostermann, A. *Int. J. Mass Spectrom.* **2010**, *295*, 72.

(57) Laurence, T. A.; Chromy, B. A. *Nat. Methods* **2010**, *7*, 338.

(58) Saenger, K. L. *J. Chem. Phys.* **1981**, *75*, 2467.

(59) Saenger, K. L.; Fenn, J. B. *J. Chem. Phys.* **1983**, *79*, 6043.

(60) Christen, W.; Rademann, K.; Even, U. *J. Chem. Phys.* **2006**, *125*, 174307.

(61) Christen, W.; Rademann, K. *Phys. Scr.* **2009**, *80*, 048127.